A Novel Silver Molybdenum Oxyfluoride Perovskite as a Cathode Material for Lithium Batteries

W. Tong,*[,†] W.-S. Yoon,[‡,§] N. M. Hagh,[†] and G. G. Amatucci[†]

Energy Storage Research Group, Department of Materials Science and Engineering, Department of Biomedical and Medical Engineering, Rutgers, The State University of New Jersey, North Brunswick, New Jersey 08902, and Brookhaven National Laboratory, Upton, New York 11973

Received December 9, 2008. Revised Manuscript Received March 11, 2009

Novel electroactive nanostructured silver molybdenum oxyfluoride (SMOF) perovskites $Ag^{1+}{}_3$-$Mo^{6+}(O_3F_3)$ have been successfully synthesized by a mechanochemical reaction. The formation of this perovskite was investigated throughout the Ag−Mo composition range with the use of either Ag^{1+} or Ag^{2+} in the form of AgF and AgF_2 as the reactant, respectively. The compositional study combined with X-ray diffraction and extensive Raman investigation was utilized to determine structure and cation distribution and infer oxidation state. Finally, preliminary electrochemical characterization of the perovskites vs lithium was investigated.

1. Introduction

A definitive focus is being made to develop cathode materials of higher energy for primary and rechargeable lithium batteries. These are driven by the needs of portable electronics[1] (such as laptops, mobile phones) and biomedical devices[2] (e.g., cardiac pacemakers, neurostimulators, drug delivery devices, implantable hearing devices, and cardiac defibrillators). For the latter, a different set of performance priorities are required, namely, energy density vs specific energy, voltage above 3 V, and long-term reliability.[3] In addition, the cost of the materials is usually a small percentage of the overall system cost and is therefore of low priority. Presently, these needs are being met by materials such as silver vanadium oxides (SVO) for higher rate applications such as defibrillators, carbon poly fluorides, and the Li−I_2 system for pacing applications. However, there is a need for new approaches to higher performance materials. For applications such as defibrillation, high energy in the voltage region above 3 V is of particular importance. There are only a few materials capable of such performance requirements, such as the well-known AgV_2O_5 and its oxyfluoride derivatives.[4]

Recently, there has been a renewed interest by a few groups in the revival of metal fluorides as high-energy-density electrode materials. The general conversion reaction of lithium batteries using transition metal fluorides as cathodes is

$$n\mathrm{Li} + \mathrm{MF}_n \leftrightarrow \mathrm{M} + n\mathrm{LiF}$$

Because of the poor electronic conductivity of these high band gap insulators, transition metal fluorides have been precluded as one of the potential cathode candidates for rechargeable lithium batteries. This is despite a relatively active period of investigation 3−4 decades ago. In a revival of this effort, our group has successfully shown the potential for near-theoretical conversion electrochemical activity at room temperature of the insulating metal fluorides (BiF_3,[5] FeF_3,[6−8] CuF_2[9]) through the use of nanocomposites utilizing single and mixed conducting matrices.

Superior to CuF_2 (8.25 W h/cc) and CF_1 (6.79 W h/cc), which deliver capacities at voltages of barely 3 V, AgF and AgF_2 are of interest because of their theoretical higher output voltages (4.16 and 4.46 V) and energy densities (6.21 and 9.1 W h/cc), respectively. In addition, silver fluoride offers the potential to enhance both the ionic and electronic conductivity compared to other transition metal fluorides in the context of (1) Ag^+ ion diffusion[10] and (2) the formation of highly conducting Ag metal with e^- transfer during discharge, respectively. Evidence of the enhanced conductivity of either cathode materials ($LiCoO_2$,[11] $LiFePO_4$[12,13]) or anode materials (TiO_2 nanotube,[14] silicon,[15] $Li_4Ti_5O_{12}$,[16,17]

* Corresponding author.
† Rutgers.
‡ Brookhaven National Laboratory.
§ Present address: Yonsei University, Seoul 120-749.

(1) Brodd, R. J.; Bullock, K. R.; Leising, R. A.; Middaugh, R. L.; Miller, J. R.; Takeuchi, E. *J. Electrochem. Soc.* **2004**, *151*, K1.
(2) Holmes, C. F. *J. Power Sources* **2001**, *97−98*, 739.
(3) Sorensen, E. M.; Izumi, H. K.; Vaughey, J. T.; Stern, C. L.; Poeppelmeier, K. R. *J. Am. Chem. Soc.* **2005**, *127*, 6347.
(4) Sauvage, F.; Bodenez, V.; Vezin, H.; Albrecht, T. A.; Tarascon, J.-M.; Poeppelmeier, K. P. *Inorg, Chem.* **2008**, *47*, 8464.
(5) Bervas, M.; Badway, F.; Klein, L. C.; Amatucci, G. G. *Electrochem. Solid-State Lett.* **2005**, *8*, A179.
(6) Badway, F.; Pereira, N.; Cosandey, F.; Amatucci, G. G. *J. Electrochem. Soc.* **2003**, *150*, A1209.
(7) Plitz, I.; Badway, F.; Al-Sharab, J.; DuPasquier, A.; Cosandey, F.; Amatucci, G. G. *J. Electrochem. Soc.* **2004**, *152*, A307.
(8) Badway, F.; Cosandey, F.; Pereira, N.; Amatucci, G. G. *J. Electrochem. Soc.* **2003**, *150*, A1318.
(9) Badway, F.; Mansour, A. N.; Pereira, N.; Al-Sharab, J.; Cosandey, F.; Plitz, I.; Amatucci, G. G. *Chem. Mater.* **2007**, *19*, 4129.
(10) Raaen, A. M.; Svare, I.; Fjeldly, T. A. *Phys. Rev. B* **1980**, *21*, 4895.
(11) Huang, S.; Wen, Z.; Yang, X.; Gu, Z.; Xu, X. *J. Power Sources* **2005**, *148*, 72.
(12) Croce, F.; D'Epifanio, A.; Hassoun, J.; Deptula, A.; Olczac, T.; Scrosati, B. *Electrochem. Solid-State Lett.* **2002**, *5*, A47.
(13) Park, K. S.; Son, J. T.; Chung, H. T.; Kim, S. J.; Lee, C. H.; Kang, K. T.; Kim, H. G. *Solid State Commun.* **2004**, *129*, 311.
(14) He, B.; Dong, B.; Li, H. *Electrochem. Commun.* **2007**, *9*, 425.

10.1021/cm803322d CCC: $40.75
Published on Web 04/22/2009

polycrystalline $LiNbO_3$[18]) have been identified with Ag and/or Cu metal additive. However, our initial efforts to stabilize AgF and AgF_2 through the composite approach did not bring about appreciable performance.

Beyond composites, it would be most ideal to develop a nanostructured material that contained appreciable mixed conductivity along with the attributes of AgF_x. In this respect, the perovskite structure (ABX_3) is of interest as a framework structure, as it can tolerate a large differential in ionic sizes between A and B, potentially opening the door to the use of silver and a wide variety of first- and second-row transition metals. In addition, such structures can support A-, B-, X-deficiency such that it potentially has available sites and conduction passes for lithium ions to occupy and to migrate.[19] In this paper, we report in detail a new perovskite-type silver molybdenum oxyfluoride (SMOF) with a general formula $Ag^{+}{}_3Mo^{6+}(O_zF_{6-z})$.[20] SMOF perovskites were successfully synthesized by the application of mechanochemistry through the use of AgF, AgF_2 and MoO_3, MoO_2 precursors.

2. Experimental Section

2.1. Silver Molybdenum Oxyfluoride Synthesis. Reagent-grade AgF_2 (Aldrich, 98+%) or AgF (Aldrich, 99%) and MoO_3 (Alfa Aesar, 99.95%), MoO_2 (Alfa Aesar, 99%) were utilized as starting materials to prepare silver molybdenum oxyfluoride (SMOF) by high energy milling. To obtain a homogeneous precursor of the initial powders, we preground stoichiometric mixtures of AgF_2/AgF and MoO_3/MoO_2 in an agate mortar for about 10 min in a He-filled glovebox.

2.1.1. High Energy Milling. One gram of the designated stoichiometric mixture was placed inside a milling cell along with milling media, both of which were made of hardened steel. To minimize any contamination resulting from handling the powders in the atmosphere, we carried out all the assemblies in a He-filled glovebox (dew point −80 °C). The milling was performed in a SPEX 8000 mixer mill for the designated time, 45min. X-ray fluorescence (XRF) was utilized to check the quantity of Fe contamination after high energy milling, which was found to be minimal (1.3 wt %) based on extrapolation to external standards.

2.2. Physical Characterization. *2.2.1. X-ray Powder Diffraction (XRD).* X-ray diffraction patterns were recorded at 0.8°/min between 15 and 65° using a Scintag X2 diffractometer with Cu Kα radiation. In the glovebox, the materials were placed on a glass slide and covered with Kapton film sealed by a layer of vacuum grease around the perimeter. For Rietveld refinement, XRD data were collected in the 2θ range of 15−80° with a step size of 0.03° and exposure of 20 s. To minimize the nondesirable system-based X-ray scatter from reaching the detector, we utilized a sample holder (The Gem Dugout) made from Si (510) mounted 50 μm below the reference surface of an Al block. The characterization of the new phase was assisted by CaRine v3.1, and the Rietveld refinement was carried out with MDI Jade v 8.0.

2.2.2. X-ray Absorption Spectroscopy (XAS). XAS measurements were performed in the transmission mode at beamline 18B of the National Synchrotron Light Source (NSLS) using a Si(111) channel cut monochromator. The monochromator was detuned to 10% of its original intensity to eliminate the high-order harmonics. Energy calibration was carried out using the first inflection point of the spectrum of Mo metal foil as a reference (i.e., Mo K-edge = 19999 eV). To remove an energy shift problem, the X-ray absorption spectrum for Mo metal foil was measured simultaneously in every measurement as the metal foil was positioned in front of the window of the third ion chamber.

2.2.3. Elemental Analysis. Elemental analysis was performed in Galbraith Laboratories, Inc. The analysis on the metal element (Ag and Mo) was conducted by inductively coupled plasma atomic emission spectroscopy (ICP-AES) and the fluorine content was analyzed by oxygen flash combustion and ion-selective electrode.

2.2.4. Raman Spectroscopy. Raman spectroscopy was conducted on an Enwave EZRaman-L series Raman system with excitation light of laser 670 nm wavelength (Enwave optronics, Inc.). The samples were measured in the range of 100−2000 cm^{-1}. In an effort to minimize the contamination of air or moisture, the samples were sealed in a specially designed cell with a laser transparent quartz window under a He atmosphere. All the measurements were conducted in a dry room (room temperature 25 °C, humidity <2%).

2.3. Electrochemical Characterization. Electrochemical characterization of the as-fabricated SMOF perovskites was performed vs Li metal (Johnson Matthey) in 2025 type coin cells with Al-clad stainless positive electrodes (Hosen Corp.). Cathodes were introduced by using either pure SMOF powder, manually mixed 80% SMOF powder, 10% SP carbon black, and 10% poly(vinylidene fluoride-co-hexafluoropropylene) (Kynar 2801, ElfAtochem) binder (wt %) or SMOF + C tape. The SMOF+C tape was prepared by casting an acetone-based slurry consisting of 57% SMOF, 12% carbon, and 31% poly(vinylidene fluoride-co-bexafluoropropylen) binder dispersed in dibutyl phthalate. The tape was then extracted using 99.8% diethyl ether (Aldrich). Within the coin cell, the electrodes were separated by a layer of Celgard separator and Whatman GF/D glass fiber separators saturated in the electrolyte consisting of 1 M $LiPF_6$ in ethylene carbonate: dimethyl carbonate (EC:DMC, 1:1 by volume) (Ferro). All the cells were assembled under He (better than −80 °C dewpoint) atmosphere and cycled at constant current 7.58 mA/g between 4−2 V at 22 °C using a MacPile galvanostat (Biologic, Claix, France), unless noted otherwise.

3. Results and Discussion

3.1. Structure: Diffraction. *3.1.1. Mechanochemical Method.* $xAgF:(1-x)MoO_3$. AgF and MoO_3 were manually premixed in stoichiometric ratios prior to high energy milling (HEM). Figure 1 shows the resulting XRD patterns of the as-fabricated materials. The initial orthorhombic MoO_3 and cubic AgF phases were eliminated during the HEM process. As shown in Figure 1, small X-ray diffraction peaks were observed for the lower percentages of AgF ($x \leq 50$ mol %). Examination of these Bragg diffractions after further crystallization by heat treatment (not shown in this paper) suggests a yet to be identified new phase that we denote as (Ag, Mo, O, F). Increasing the AgF content to 60 mol % or higher resulted in the formation of dominant Bragg reflections at approximately 2.92, 2.06, 1.68, 1.46, and 1.30 Å, revealing a significant new phase that we denote as SMOF from this point on. This phase is a departure from the MoO_3 and AgF precursors and remained as the significant phase in a wide range of AgF−MoO_3 compositions ($x = 60-80$). Very small

(15) Yang, X.; Wen, Z.; Huang, S.; Zhu, X.; Zhang, X. *Solid State Ion.* **2006**, *177*, 2807.
(16) Huang, S.; Wen, Z.; Zhang, J.; Yang, X. *Electrochim. Acta* **2007**, *52*, 3704.
(17) Huang, S.; Wen, Z.; Zhang, J.; Gu, Z.; Xu, X. *Solid State Ionics* **2006**, *177*, 851.
(18) Son, J. T. *Electrochem. Commun.* **2004**, *6*, 990.
(19) Shan, Y. J.; Chen, L.; Inaguma, Y.; Itoh, M.; Nakamura, T. *J. Power Sources* **1995**, *54*, 397.
(20) Tong, W.; Amatucci, G. G. *ECS Trans.* **2008**, *11*, 19–25.

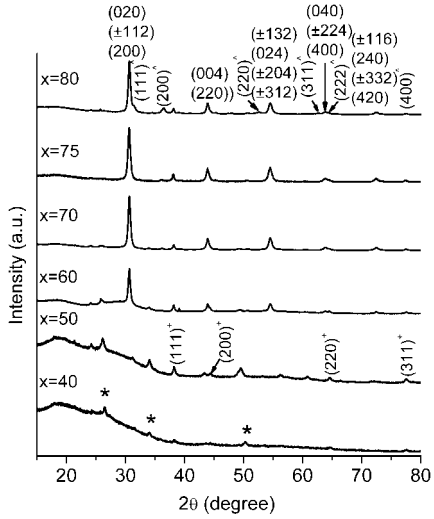

Figure 1. XRD patterns of mechanically milled xAgF:$(1-x)$$MoO_3$ for 45 min in a He atmosphere. SMOF perovskite, Ag, and AgF indices are denoted by (hkl), $(hkl)^+$, and (hkl)^, respectively. (Ag, Mo, O, F) phase is indicated by *. For SMOF perovskite, only relatively strong Bragg peaks are marked.

Table 1. Observed *d*-Spacing and Indexing of the As-Fabricated SMOF Perovskite (75 mol% AgF) Based on a Cubic Unit Cell[a]

hkl	d_{obsd} (Å)	d_{calcd} (Å)	$(d_{obsd} - d_{calcd})$
220	2.916	2.915	1×10^{-3}
400	2.061	2.061	0
422	1.683	1.683	0
440	1.458	1.457	1×10^{-3}
062	1.304	1.304	0

[a] $a = b = c = 8.245 \pm 1 \times 10^{-3}$ (Å), $V = 560.46$ (Å^3).

amounts of second phases consisting of Ag or AgF were also present in the diffraction patterns in this composition range. At 75 mol % AgF, the SMOF phase reached an intensity maximum with minimal quantity of Mo- or Ag-containing minor phases. When AgF content was below 75 mol %, the minor phase was characterized to be consistent with the unknown (Ag, Mo, O, F) phase. In contrast, high AgF loading (80 mol %) resulted in an excess of Ag content in the form of AgF and Ag with the absence of residual Mo phases.

The initial refinement and resulting indexing (Table 1) of the XRD pattern of the dominant new phase was performed on the relatively pure 75 mol % sample. The phase was originally indexed well to be a cubic structure, suggesting a crystal of perovskite origin. Perovskites are known to be stable structures for a number of metal oxyfluorides. The extended perovskite structure family includes the structures of the classical perovskite ABX_3 in which A (cation) is located at the center of the cubic unit cell, B (cation) is located at each corner, and X (anions) are located at the center of each side; distorted ABX_3 perovskite; ordered perovskite ($A_2BB'X_6$); layered perovskite (Ruddlesden−Popper ($A_{n+1}B_nX_{3n+1}$), Dion−Jacobson ($A'[A_{n-1}B_nX_{3n+1}]$); Aurivillius ($(Bi_2O_2)[A_{n-1}B_nX_{3n+1}]$) and $A_nB_nX_{3n+2}$, $A_{n+1}B_nX_{3n+3}$; elpasolite ($A_2BB'X_6$); cryolite perovskite (A_3BX_6), and other perovskite structures.[21]

(21) Mitchell, R. H. *Perovskites: Modern and Ancient*; Almaz Press Inc.: Thunder Bay, ON, Canada, 2002.

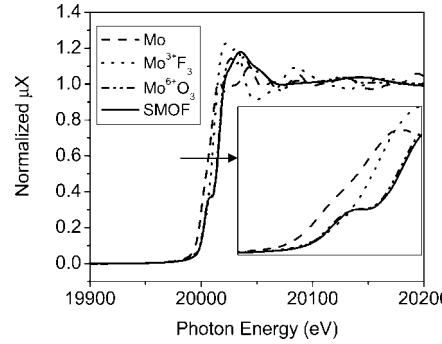

Figure 2. XANES spectra comparing Mo in the as-fabricated SMOF phase vs that of Mo^{3+}-, Mo^{6+}-containing standards.

Table 2. Elemental Analysis Results of the SMOF Samples Fabricated by Both Ag^+F and $Ag^{2+}F_2$

element	(wt %)	(mol %)	molar ratio of Ag/F to Mo	experimental molecular formula (charge balance)
			SMOF (AgF, $x = 75$)	
Ag	60.0	0.5562	3.07	$Ag^+_{3.07}Mo^{6+}_1O_{3.16}F_{2.75}$
Mo	17.4	0.1814	1	
F	9.48	0.4989	2.75	
			SMOF (AgF_2, $x = 75$)	
Ag	58.9	0.5460	3.19	$Ag^+_{3.19}Mo^{6+}_1O_{2.335}F_{4.52}$ $Ag^+_{3.19}Mo^{4+}_1O_{1.335}F_{4.52}$
Mo	16.4	0.1709	1	
F	14.68	0.7726	4.52	

Before the structure was examined further, analysis was performed to determine the oxidation state of the Mo. Assuming that Ag^{1+} is the stable oxidation state incorporated within the new phase, the perovskites, with a mixed O/F anion composition, offer a variety of stoichiometric opportunities to form with the reduced oxidation states of Mo. The electronic modification of the as-fabricated perovskite phase was examined by XANES through XAS. XANES was performed on the SMOF fabricated by AgF at $x = 0.7$ based on the purity of the sample (close to the optimum 0.75 ratio) and the good electrochemistry discussed later in this paper. A comparison of the Mo K-edge XANES data for SMOF along with Mo, $Mo^{3+}F_3$, $Mo^{6+}O_3$ reference compounds is shown in Figure 2. As shown in Figure 2, the Mo K-edge spectra of the various compounds show a positive energy shift with an increase in formal valency and the energy at half-height for SMOF is perfectly consistent with that for $Mo^{6+}O_3$, indicating the valence state of Mo in the as-fabricated perovskite is +6. On the basis of cation occupation and charge balancing, the classic perovskite structure ABX_3 ($X = O^{2-}$ or F^-) was excluded by the XANES results.

The structure determination of the perovskite phase was pursued on the basis of two facts: (1) the valence state of Mo within the perovskite phase is +6 and (2) the relatively pure perovskite phase developed consistently and reproducibly at 75 mol % AgF composition. The stoichiometry of Ag:Mo = 3:1 leads to the natural conclusion that this phase is of the cryolite-type perovskite stoichiometry (A_3BX_6). This is further confirmed by the results of the Ag, Mo, and F elemental analysis (Table 2). The calculated O content is based on the charge balancing. For SMOF materials fabricated with AgF_2, the presence of Mo^{4+} was indicated by

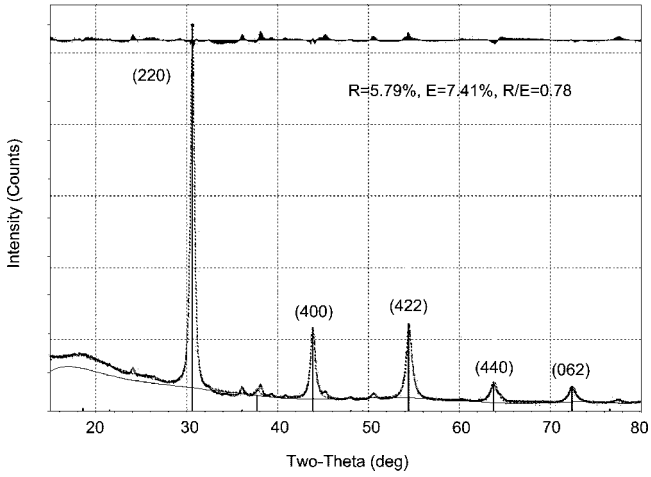

Figure 3. Observed (circles) and calculated (continuous line) X-ray diffraction profiles of $Ag_3MoO_3F_3$ with cryolite-type structure (*Fm3m*). The overlaying vertical lines indicate the expected Bragg reflections. On the top, the difference plot, $I_{obsd} - I_{calcd}$, is shown. The refinement was based on SMOF (AgF, $x = 75$).

Raman spectroscopy (as discussed later); therefore, the calculation of the experimental molecular formula is based on either Mo^{4+} or Mo^{6+}. As shown in Table 2, the experimental molecular formula ($Ag^{+}_{3.07}Mo^{6+}_{1}O_{3.16}F_{2.75}$) of AgF-based SMOF is very close to the stoichiometric $Ag^{1+}_{3}Mo^{6+}_{1}X_6$ corresponding to the cryolite structure.

Cryolite is a particular case of elpasolite structure $A_2BB'X_6$, in which two kinds of nonequivalent ionic BX_6 and $B'X_6$ octahedra are linked by X atoms. For cryolite structure, A and B are chemically identical, in which atoms A occupy half of the octahedral and all dodecahedra sites. At this point, for discussion purposes, we denote the new phase as Ag_3MoX_6. To confirm this identification, Rietveld analysis on the XRD data of high-energy-milled 75 mol % AgF: 25 mol % MoO_3 was initially performed on the basis of the *Fm3m* space group symmetry. As shown in Figure 3, it seems a good fitness was indicated by $R = 5.79\%$, $E = 7.41\%$, $R/E = 0.78$ between the observed X-ray diffraction pattern (circled) and the calculated profile (continuous line) based on the *Fm3m* cryolite. However, close examination revealed a poor fitness of several very small Bragg peaks that are present on the observed XRD pattern.

Structural conclusions were further investigated by the well-known radius ratios rules and tolerance factor, for the stabilization and occupation of allowed sites within the perovskite structure based on the ionic radius of the constituent atoms. For the classic perovskite structure ABX_3, the tolerance factor t gives an indication of how far from the ideal packing induced by the relative size of the A, B, and X ions can be tolerated.[22] This is described in the formula

$$t = (r_A + r_X)/\sqrt{2}(\langle r_B \rangle + r_X) \quad (1)$$

Where r_A, $\langle r_B \rangle$ are the average radii of the cations on A, B sites respectively, r_X is the anion radius on X site.[23] The octahedral factor assures the stability of BX_6 octahedron, and in turn, the stability of perovskite structure. More specially, the modified Goldschmidt's tolerance factor is very important to define the stability of the cryolite-type structure. For the elpasolite ($A_2BB'X_6$) crystal structure, the modified Goldschmidt's tolerance factor t is described as[24]

$$t = \sqrt{2}(r_A + r_X)/(r_B + r_{B'} + 2r_X) \quad (2)$$

where r_A, r_B, $r_{B'}$, and r_X are the radii of A, B, B′ and X ions for the elpasolite-type structure. The tolerance factor of the Ag_3MoX_6 cryolite composition is 0.81. Usually, a cubic structure is stable for the compounds with large tolerance factor close to unity. This low tolerance factor along with the unmatched small Bragg reflections based on *Fm3m* cubic symmetry leads to the conclusion that the as-fabricated silver molybdenum oxyfluoride may have lower symmetry. Therefore, a refinement based on a monoclinic perovskite-related structure was performed in order to improve the fitting of the small reflections. With referring to the monoclinic $P2_1/n$ (No. 14 or C^5_{2h}) space group, a good fitness was indicated by $R = 3.69\%$, $E = 7.38\%$, $R/E = 0.5$ (Figure 4), with all the small reflections matched. The refined structural parameters of $Ag_3MoO_3F_3$ are given in Table 3. A conclusive determination of the space group would be best performed with single-crystal diffraction, which is outside the scope of this paper.

3.1.2. Effect of Alternative Precursor. $xAgF_2:(1-x)MoO_3$. Because of the combination of higher oxidative power and fluorine content, it was of interest to investigate the formation of SMOF perovskite by using the alternative precursor AgF_2. We performed high-energy milling of $xAgF_2:(1-x)MoO_3$ mixtures to study the influence of AgF_2. The experiments were conducted identically to those previously stated for the AgF samples. Figure 5 shows the XRD patterns of high-energy-milled $xAgF_2:(1-x)MoO_3$ with AgF_2 loadings ranging from 50 to 80 mol %. As shown in Figure 5, an X-ray diffraction amorphous phase was obtained when 50 mol % AgF_2 and 50 mol % MoO_3 were milled. X-ray diffraction patterns were also X-ray amorphous for all the lower percentages of AgF_2 ($x < 50$ mol %); these are not shown for the sake of figure clarity. With the AgF_2 content increasing to 60 mol % or higher, dominant Bragg peaks developed at approximately 2.91, 2.06, 1.68, and 1.46 Å, indicating the formation of SMOF perovskite phase, which was similar to what was observed in the case of AgF. An exception was present in the XRD pattern of the 70 mol % sample. At this percentage, a distinct Bragg peak of significant intensity developed around 3.23 Å along with the Bragg peaks observed for the other compositions. To investigate if these peaks are of a second phase or a lattice distortion of the main phase, an XRD result of a very long scan was given in Figure 5, revealing a significant number of Bragg reflections. Examination of the behavior of the phase and indexing suggests that it is indeed a lattice distortion of the main phase. The structure of this second phase was indexed to be monoclinic with lattice parameters of $a = 12.349$ (0.005), $b = 5.223$ (0.001), $c = 6.716$ (0.001) Å, $\alpha = \gamma = 9°$, $\beta = 91.56°$, and $V = 433.5$ Å^3. Seventy-

(22) Bhalla, A. S.; Guo, R.; Roy, R. *Mater. Res. Innovations* **2000**, *4*, 3.
(23) Moustafa, A. M.; Ahmed Farag, I. S.; Salah, L. M. *Egypt. J. Solids* **2004**, *27*, 213.
(24) Flerov, I. N.; Gorev, M. V.; Aleksandrov, K. S.; Tressaud, A.; Grannec, J.; Couzi, M. *Mater. Sci. Eng.* **1998**, *24*, 84.

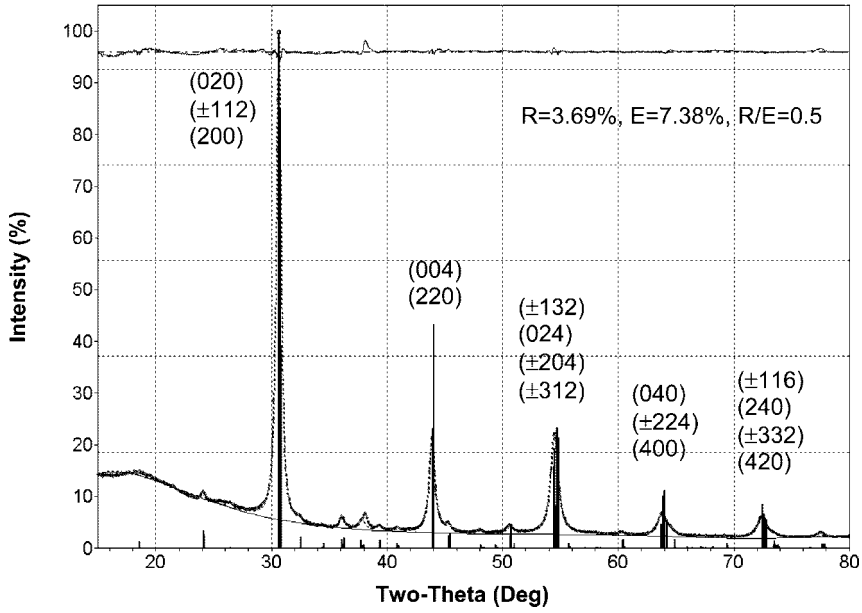

Figure 4. Observed (crosses) and calculated (continuous line) X-ray diffraction profiles of $Ag_3MoO_3F_3$ with monoclinic $P2_1/n$ (No. 14 or C^5_{2h}) perovskite structure. The overlaying vertical lines indicate the expected Bragg reflections. On the top, the difference plot, $I_{obsd} - I_{calcd}$, is shown. The refinement was based on SMOF (AgF, $x = 75$). Only relatively strong Bragg diffractions are marked.

Table 3. Refined Structural Parameters of $Ag_3MoO_3F_3$ Based on $P2_1/n$ (No. 14 or C^5_{2h}) Space Group[a]

atom	Wyckoff	*x*	*y*	*z*	occupancy (*n*)
Ag1	4	0.01428	0.02946	0.7574	1
Ag2	2	0.5	0	0	0.8532
Mo	2	0.5	0	0.5	0.9019
O/F	4	0.3055	0.2869	0.8964	0.5
O/F	4	0.2637	0.3199	0.4922	0.5
O/F	4	0.9254	0.4808	0.7944	0.5

[a] Space group: $P2_1/n$ (14) <b-unique>, $a = 5.8075$, $b = 5.8416$, $c = 8.2535$, $\alpha = \gamma = 90°$, $\beta = 90.20°$, $R = 3.69\%$, $E = 7.38\%$, $R/E = 0.5$.

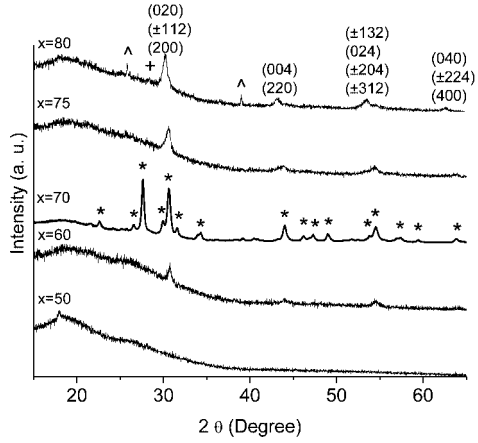

Figure 5. XRD patterns of $xAgF_2:(1-x)MoO_3$ (mol %) formed by high energy milling for 45 min in a He atmosphere. SMOF perovskite indices are denoted by (*hkl*), * marks another monoclinic SMOF phase, + and ^ refer to AgF_2 and MoO_3 phase, respectively. Only relatively strong Bragg diffractions of SMOF perovskite are marked.

five mole percent AgF_2 led to a phase-pure material, whereas increasing the amount to 80 mol% led to small amounts of unreacted AgF_2 and MoO_3 residuals.

Interestingly, it can be seen in Figure 5 that the relative intensities of the perovskite Bragg reflections did not change as the compositions of the samples varied above 60 mol % AgF_2. However, the significant shift to larger lattice parameter with $Ag^{2+}F_2$ content in this region is observed. To investigate if this was a simple lattice expansion or a structure change, Rietveld refinement was performed based on the XRD of the ideal stoichiometry (75 mol % AgF_2) with referring to $P2_1/n$. This sample was from a subsequent batch of materials and the XRD pattern was a result of a very long scan. As shown in Figure 6, the goodness of fit ($R = 4.04\%$, $E = 7.52\%$, $R/E = 0.54$) indicated that this was indeed of a monoclinic space group, and the significant peak shift is consistent with Vegard's rule for the substitution of a larger cation (Figure 7). The observed expansion of the unit cell can be explained in two ways. On the one hand, it could be due to the substitution of the large Ag^{2+} (0.89 Å) for Mo^{6+} (0.62 Å) ion with increasing $Ag^{2+}F_2$ content. More likely, smaller Mo^{6+} (0.62 Å) may be partially reduced to larger Mo^{4+} (0.7 Å) on B sites in the cubic lattice with the increase in fluorine on the sublattice. This reduction process would be consistent with a rapid increase in F content at the higher substitution percentage, which was indicated by the elemental analysis. Besides the lack of expansion observed for compounds utilizing $Ag^{1+}F$ as a precursor (Figure 7), the gradual incorporation of Mo^{4+} on the B sites for all compositions >50 mol % seems to be supported by the results of Raman spectroscopy, which will be presented below in detail. Oxidation state of anion composition and detailed structural determination for all the compositions is beyond the scope of this paper and will be discussed in a later publication.

3.1.3. Annealing of the Nanoperovskites. The nanoperovskite samples prepared by HEM of $xAgF_2:(1-x)MoO_3$ were annealed under Ar for 2 h at 200 °C to crystallize to a greater extent to aid interpretation. The low temperature was chosen to limit decomposition of the fluoride. The resulting XRD patterns are shown in Figure 8. In short, the application of thermal energy resulted in the further crystallization of the perovskite phases observed at 60 mol % AgF_2 and above with little decomposition. In no way did the thermal treatment result in the crystallization of the previously amorphous

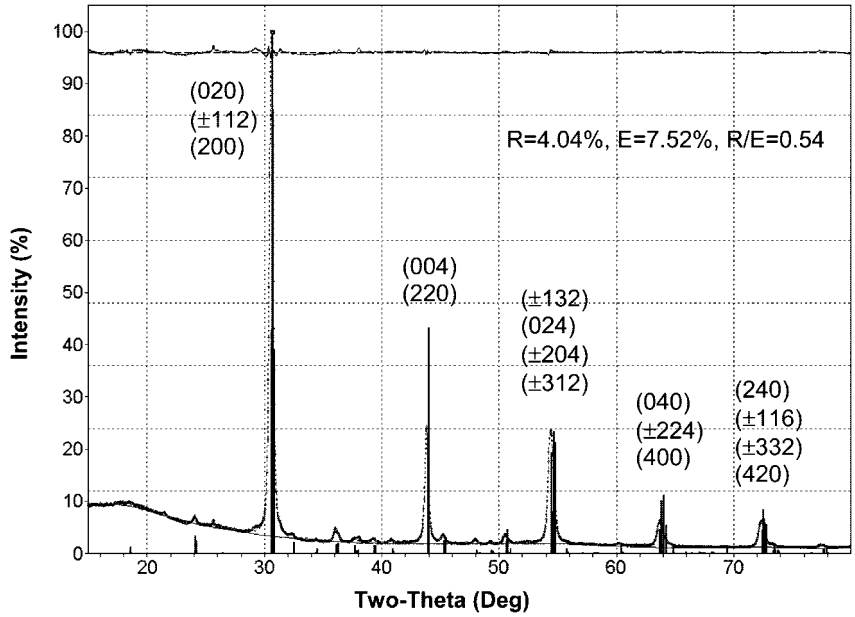

Figure 6. Observed (crosses) and calculated (continuous line) X-ray diffraction profiles of $Ag_3MoO_3F_3$ with monoclinic $P2_1/n$ (No. 14 or C^5_{2h}) perovskite structure. The overlaying vertical lines indicate the expected Bragg reflections. On the top, the difference plot, $I_{obsd} - I_{calcd}$, is shown. The refinement was based on SMOF (AgF_2, $x = 75$). Only relatively strong Bragg diffractions of SMOF are labeled.

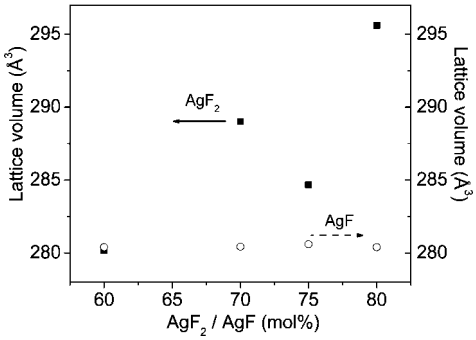

Figure 7. Lattice volumes of monoclinic perovskite phases of various Ag precursors synthesized by mechanochemistry, $xAgF_2:(1-x)MoO_3$; xAgF:$(1-x)MoO_3$.

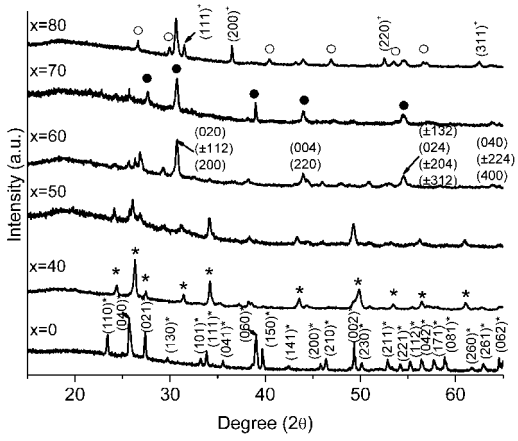

Figure 8. XRD patterns of annealing mechanochemically synthesized phases $xAgF_2:(1-x)MoO_3$ (mol %) in Ar at 200 °C for 2 h. SMOF perovskite, MoO_3, and AgF indices are denoted by (hkl), (hkl)*, and $(hkl)^+$, respectively. Another monoclinic SMOF and (Ag, Mo, O, F) phase are indicated by • and *, Mo_8O_{23} is marked by □. Only relatively strong Bragg diffractions of SMOF are marked.

samples present at AgF_2 percentages less than 60 mol % to a perovskite phase. In contrast, phases related to MoO_3 and a new phase (denoted as (Ag, Mo, O, F)), yet to be identified,

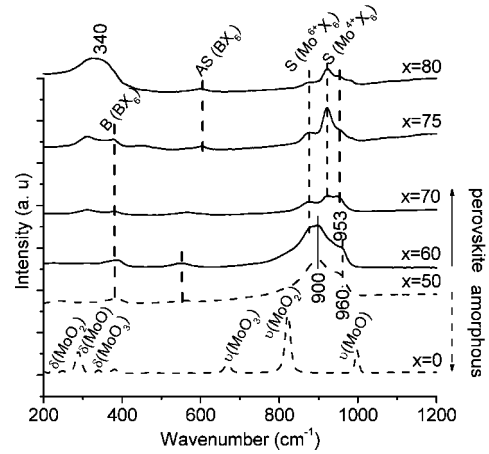

Figure 9. Raman spectra of mechanically milled $xAgF_2:(1-x)MoO_3$ (mol %) for 45 min in a He atmosphere.

were seen to develop in this region. Therefore, the X-ray amorphous phases for compositions less than 60 mol % did not seem to consist of poorly crystallized, X-ray amorphous perovskite phase. This is a conclusion that will be reinforced by Raman characterization discussed below.

3.2. Structure: Raman Spectroscopy. The structure of the as-fabricated silver molybdenum oxyfluoride was further investigated by Raman spectroscopy for its usefulness in the further determination of perovskite structure.[25] The Raman spectra of as-fabricated SMOF perovskites are plotted in Figures 9−11 as a function of AgF_2 content in the compositions. As shown in Figure 9, the spectrum of an α phase crystalline MoO_3 is mainly characterized by four sharp Raman peaks at 997 (υ(OMo)), 820 (υ(OMo_2)), 668 (υ(OMo_3)), and 288 cm^{-1} (δ(OMo)).[26,27] The absence of the

(25) Dias, A.; Khalam, L. A.; Sebastian, M. T.; Moreira, R. L. *J. Solid State Chem.* **2007**, *180*, 2144.
(26) Lee, S.; Seong, M. J.; Tracy, C. E.; Mascarenhas, A.; Pitts, J. R.; Deb, S. K. *Solid State Ionics* **2002**, *147*, 129.

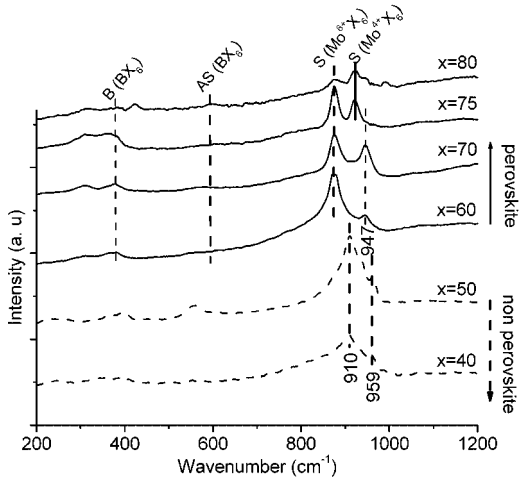

Figure 10. Raman spectra of annealing mechanically milled xAgF$_2$:(1−x)MoO$_3$ (mol %) in Ar at 200 °C for 2 h.

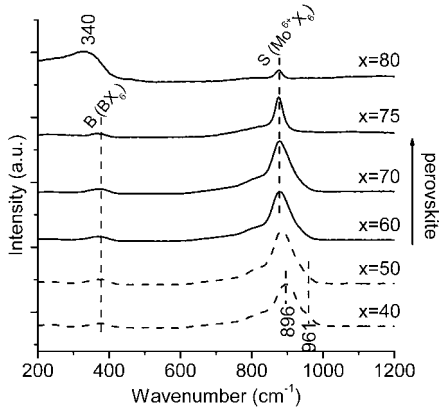

Figure 11. Raman spectra of mechanically milled xAgF:(1−x)MoO$_3$ (mol %) for 45 min in a He atmosphere.

characteristic peaks of MoO_3 clearly indicates that MoO_3 does not exist as a nearly X-ray amorphous nano phase in any of the compositions. Raman identification of AgF_2 was not possible at the utilized wavelength because of its high fluorescence.

The common features of the resulting spectra were the bands in the range of 940−960, 920−925, 900, and 876 cm^{-1} and a group of weak peaks around 383, 340, and 315 cm^{-1}. The strong band around 900 cm^{-1} was observed at relatively low AgF_2 loadings (≤60 mol %), which associates with the X-ray amorphous phase. With AgF_2 content increasing to 60 mol% and above, a Raman peak developed around 876 cm^{-1}. At very high AgF_2 loading (∼75 mol %), the characteristic band was observed around 920−925 cm^{-1} at the expense of 876 cm^{-1} component. In the low-frequency region, the coalescence of two weak peaks around 315 and 383 cm^{-1} into a broad 340 cm^{-1} band was observed at very high AgF_2 content (∼80 mol %). As discussed in detail below, the 876 cm^{-1} peak observed at mid % is believed to be characteristic of the $Mo^{6+}X_6$ in the SMOF perovskite and the 925−920 cm^{-1} component is associated with the insertion of Mo^{4+} in $Mo^{6+}X_6$ octahedra.

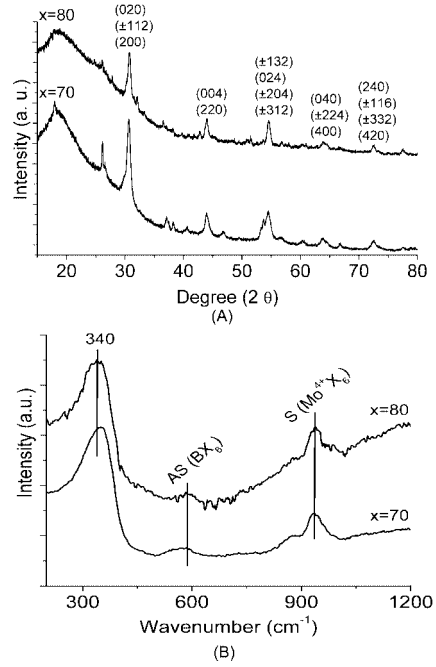

Figure 12. (A) XRD and (B) Raman spectra of SMOF perovskites fabricated by high-energy milling xAgF$_2$:(1−x)MoO$_2$ for 45 min (x = 70, 80). Only relatively strong Bragg diffractions of SMOF are marked.

According to the factor group analysis, 4 vibrations v_1 (A_{1g}), v_2 (E_g) and 2 v_5 (F_{2g}) are Raman-active for *Fm*3*m* space group[28] and 24 Raman modes (12 A_g+ 12 B_g) should be observed for the $P2_1/n$ structure.[25,29] Although at first glance the number of the observed modes is significantly less than 24, as expected for $P2_1/n$ structure in the Raman spectra of SMOF perovskite, a closer analysis of peak asymmetry and possible coalescence clearly reveals that more than four observed modes support the Rietveld refinement result, which indicated that the crystal structure of the as-fabricated SMOF perovskite belongs to much lower symmetry than the cubic *Fm*3*m* such as the monoclinic space group identified by XRD. The low number of observed bands can be explained by the accidental degeneracy of a number of modes or the coalescence of some bands[29] within the resolution limit of this particular Raman instrument. The latter is especially plausible with respect to the relatively weak distortion of the BX_6 octahedra in our monoclinic structure. Thus, the splitting of the degenerate modes is expected to be small, resulting in the invisibility of the newly activated peaks within our resolution limits.[30]

The former Raman studies on the ordered cubic perovskite compounds $A(B'_{1-x}B''_x)O_3$ (A = Pb, La, Ba, Sr, B' = Sc, Mg, Co, Ni, Zn, Cd, Ca, etc., B'' = Mo, W, Ta, Ti, etc.)[31−33] revealed four Raman-active peaks were observed around 800,

(27) Li, Z.; Gao, L.; Zheng, S. *Appl. Catal., A* **2002**, *236*, 163.

(28) Nakamoto, K. *Infrared and Raman Spectra of Inorganics and Coordination Compounds, Part I*; John Wiley & Sons Inc.: New York, 1997; p 214.

(29) Manoun, B; Igartua, J. M.; Gateshki, M.; Saxena, S. K. *J. Phys.: Condens. Matter* **2004**, *16*, 369.

(30) Iliev, M. N.; Abrashev, M. V.; Litvinchuk, A. P.; Hadjiev, V. G.; Guo, H; Gupta, A. *Phys. Rev. B* **2007**, *75*, 104118–2.

(31) Setter, N.; Laulicht, I. *Appl. Spectrosc.* **1987**, *41*, 526.

(32) Maczka, M.; Hanuza, J.; Fuentes, A. F.; Morioka, Y. *J. Phys.: Condens. Matter* **2004**, *16*, 2297.

(33) Levin, I.; Vanderah, T. A.; Amos, T. G.; Maslar, J. E. *Chem. Mater.* **2005**, *17*, 3273.

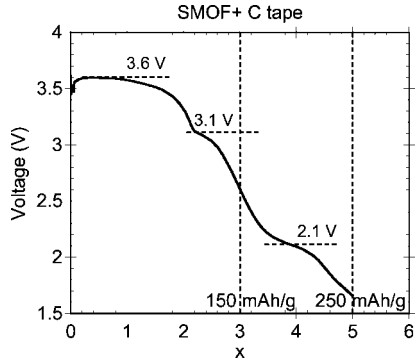

Figure 13. Voltage profile of an SMOF+C tape. The cell was cycled at 3 mA/g. x = # of Li^+ and e^- inserted into $Ag_3MoO_3F_3$ formula unit.

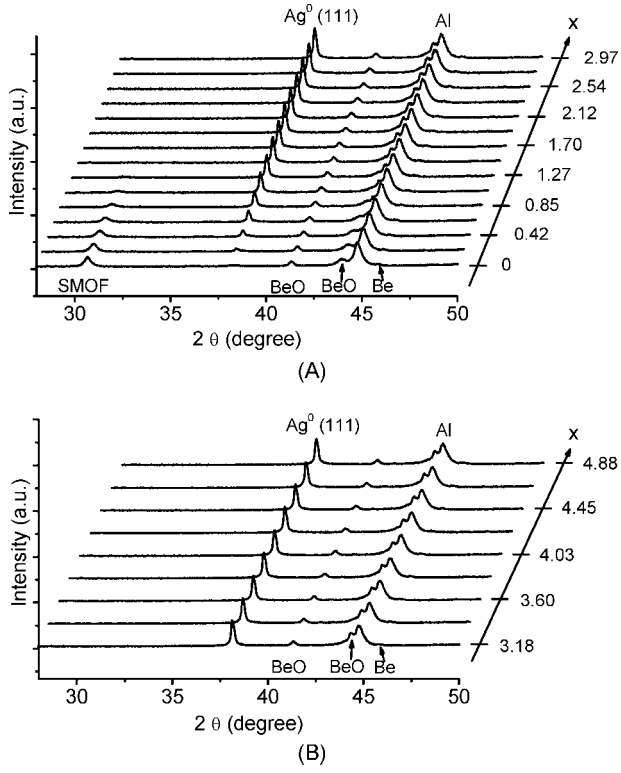

Figure 14. In situ XRD patterns of SMOF in the region (A) 4−3 V, (B) 3−1.5 V during the first discharge. x = # of Li^+ and e^- inserted into $Ag_3MoO_3F_3$ formula unit.

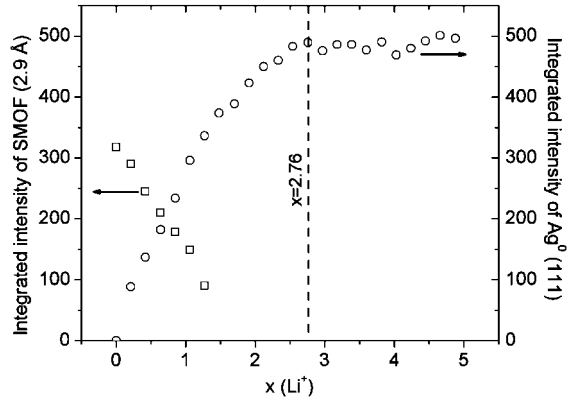

Figure 15. Integrated intensity of SMOF peaks around 2.9 Å and Ag^0 (111) peak obtained from in situ XRD patterns during discharge.

600, and 400 cm^{-1}, and lower frequency. These bands were respectively assigned to the symmetric breathing of oxygen octahedrons (A_{1g}), asymmetric breathing of oxygen octahedrons (E_g), bending of oxygen octahedrons (F_{2g}). Another lower-frequency F_{2g} vibration mode is primarily related to the displacement of A cation. In the distorted structure ($P2_1/n$), the degeneracy of E_g and F_{2g} modes are totally lifted and additional Γ-point phonons become Raman-active.[30] In the previous work on the Raman spectra of $P2_1/n$ structure, Raman bands were usually observed in the range of 100−1100 cm^{-1} and classified into three spectral regions: high-frequency bands corresponding to stretching vibrations of the BX_6 octahedra, midfrequency bands and low-frequency bands associate with antistretching and bending motions.[25,29] Both the stretching and antistretching modes originate from the Raman active modes of A_{1g} and E_g of the cubic $Fm3m$ parent structure.[34] For discussion purposes, we divide the Raman spectra of monoclinic SMOF into three families: high-frequency bands (>600 cm^{-1}), midfrequency bands (400−600 cm^{-1}), and low-frequency bands (<400 cm^{-1}), as the vibration bands in the above regions are related to A_{1g}, E_g and F_{2g} vibration modes of the cubic $Fm3m$ structure, respectively.

In short, based on the aforementioned Raman literature, we assign the peaks around 876, 600, and 383 cm^{-1} to the stretching (S), antistretching (AS), and bending (B) vibration modes of MoX_6 octahedron, respectively, where the antistretching mode (∼600 cm^{-1}) could be invisible because of its low intensity. The 925−920 cm^{-1} component was associated with the Mo^{4+}−X bond in BX_6 octahedron present in the high AgF_2 compositions. The details will be discussed for each band below.

3.2.1. Interpretation of the Raman Peak 876 cm^{-1}. The XRD analysis of the SMOF perovskites fabricated by mechanochemical approach indicated that no perovskite phase formed until the AgF_2 loading reached to 60 mol %, in contrast, an amorphous phase (non-perovskite related) was obtained at 50 mol % AgF_2 content and below. Precisely at the formation of the perovskite phase at 60 mol %, we see the parallel development of the Raman peak around 876 cm^{-1} on the corresponding Raman spectra. To further support this assignment, we collected Raman spectra (Figure 11) on the samples prepared by mechanical milling xAgF:$(1-x)MoO_3$ (mol %). Again, we saw the development of the Raman active band around 876 cm^{-1} at $x \geq 60$ for this series using pure AgF. Again, the development of this band parallels the development of the perovskite phase as indicated by XRD (Figure 1). Therefore, we assigned the Raman peak around 876 cm^{-1} to the characteristic Raman peak of SMOF perovskite phase. Consistent with the above referenced studies,[29] we can ascribe the 876 cm^{-1} Raman band to stretching vibrations of the $Mo^{6+}X_6$ octahedron.

3.2.2. Interpretation of the Raman Peak 925−920 cm^{-1}. Two observations aroused our interest in the investigation of the origin of the Raman peak around 925−920 cm^{-1}: (1) the 920−925 cm^{-1} band was observed to develop at high AgF_2 content; (2) as opposed to the Raman spectra with starting materials consisting of $Ag^{2+}F_2$, no 925−920 cm^{-1} band was observed for samples fabricated using pure AgF, even at high $Ag^{1+}F$ loading (80 mol %). The significant

(34) Iliev, M. N.; Padhan, P.; Gupta, A. *Phys. Rev. B* **2008**, *77*, 172303–2.

Table 4. Comparison of Energy Densities of Silver Molybdenum Oxyfluoride SMOF (AgF, $x = 75$) and Silver Vanadium (SVOF) Materials[a]

		C_1		E_1			C_2		E_2		E	
battery	V_1 (V)	(A h/kg)	(A h/L)	(W h/kg)	(W h/L)	V_2 (V)	(A h/kg)	(A h/L)	(W h/kg)	(W h/L)	(W h/kg)	(W h/L)
Li/SVO	3.2	91	441	291	1411	2.4	224	1080	538	2592	829	4003
Li/SMOF	3.38	123	761	416	2570	2.43	127	784	308	1904	724	4474

[a] *V*, *C*, *E* respectively refer to voltage (V), gravimetric capacity (A h/kg) and volumetric capacity (A h/L), and gravimetric energy density (W h/kg) and volumetric energy density (W h/L). The subscripts 1, 2 refer to the two voltage ranges 4−3 and 3−1.5 V.

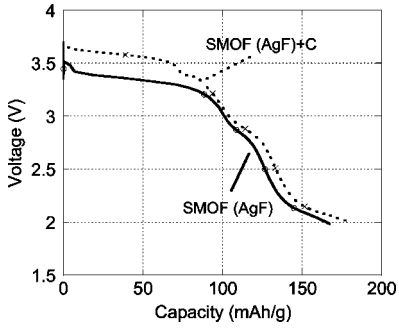

Figure 16. Voltage profiles of the SMOF perovskite. Electrodes were introduced in the form of pure SMOF powder and manually mixed 80 SMOF:10 SP:10 PVDF (wt %). SMOF was prepared by high-energy milling of 75 AgF:25 MoO_3 (mol %). Cells were cycled without carbon additive at 7.58 mA/g at room temperature vs Li metal.

variation of the 925−920 cm^{-1} Raman peak with AgF_2 strongly suggests that the 925 cm^{-1} peak is associated with a likely substitution of Mo^{4+} for Mo^{6+} at high F^- content, resulting in a second stretching vibration mode for a $Mo^{4+}X_6$ octahedron of the perovskite. The observation of the 925 cm^{-1} band also coincides nicely with the onset of the AgF_2-dependent increase in lattice volume in the XRD studies, as one would expect by Vegard's rule for the larger Mo^{4+} cation. Again, the SMOF fabricated with AgF did not show an increase in lattice volume nor the presence of a Raman band at 925 cm^{-1}. To put the question of Mo^{4+} to rest, we investigated the fabrication of SMOF using $Mo^{4+}O_2$ precursor rather than a $Mo^{6+}O_3$ precursor. As indicated by XRD (Figure 12A), it can be seen that the perovskite phase developed at $x = 70-80$ by high-energy milling $xAgF_2$:$(1-x)MoO_2$ for 45 min. At $x = 80$, the lattice volume (293.92 $Å^3$) of the SMOF perovskite using MoO_2 is very similar to that (295.51 $Å^3$) of the SMOF perovskite starting with MoO_3. Interestingly, in the Raman spectra of these perovskites (Figure 12B), the formerly identified Raman characteristic peak of SMOF perovskite (876 cm^{-1}) was absent, suggesting the absence of Mo^{6+} in the SMOF perovskite of AgF_2:MoO_2. Instead, a Raman peak was observed to develop around 930 cm^{-1}, perfectly consistent with the AgF_2 samples. In light of the instability of Mo^{3+}, it is more likely that in the SMOF perovskite of AgF_2:MoO_2, Mo^{4+} cations rather than Mo^{6+} occupy B sites and form $Mo^{4+}X_6$ octahedra. Combination of XRD and Raman characterization strongly suggests that the 925 cm^{-1} peak is more possibly associated with the presence of Mo^{4+} forming $Mo^{4+}X_6$ octahedra. According to the group theory analysis and charge balancing rule, this peak can be unambiguously assigned to the stretching vibration mode of the $Mo^{4+}X_6$ octahedron in the SMOF perovskite of AgF_2:MoO_2.

The increase in wavenumber (876 → 925 cm^{-1}) for the Mo^{4+}-substituted Mo^{6+}-based B site is somewhat counterintuitive. On the basis of the theory of molecular vibration $\upsilon \propto \sqrt{(f)/(m)}$, f is a constant related to bond strength and m is the mass, this blue shift exhibited by the substitution of Mo^{4+} for Mo^{6+} on B sites suggested that the $X-Mo^{4+}-X$ bond strength was increased compared to the $X-Mo^{6+}-X$ counterpart. With the inclusion of F^- into BX_6 octahedron at high F^- content, the shortened $F^-Mo^{4+}-F^-$ bond length could be due to the strong hybridization of Mo^{4+}-d and F^--p states, leading to the observed blue shift.[35,36]

3.2.3. Interpretation of the Raman Peak 900 cm^{-1} and 960−940 cm^{-1}. The band around 900 cm^{-1} was mainly observed in the X-ray amorphous region at relatively low AgF_x loadings ($x = 40-50$), therefore, ascribed to the above-mentioned unidentified (Ag, Mo, O, F) phase. Through a literature survey, we found that the ∼900 cm^{-1} peak was often observed in the study of MoO_3 model catalysts. The assignment of this band to the vibration of a tetrahedral MoO_x species was mentioned by Tayo Olorunyolemi et al. during the Raman studies on $NiO-MoO_3$ supported on Ga_2O_3. They also presumed that it may originate from a polymeric one consisting of tetrahedral Mo species.[37] Similar conclusion was also made by Christodoulakis et al.[38] by assigning the peaks in this region to Mo−O−Mo functionalities of Mo species. Therefore, we assign the ∼900 cm^{-1} band to the Mo−O−Mo vibration of the MoO_x species.

Paralleling the 900 cm^{-1} component, the ∼960 cm^{-1} peak appeared in the X-ray amorphous region ($x = 40-50$), independent of $Ag^{2+}F_2$ content. Hence, they are both believed to result from the amorphous phase and the yet unidentified phase that crystallized upon heat treatment. As the AgF_x content increased to the percentages within the window of SMOF perovskite formation (∼70 mol %), both the 900 and 960 cm^{-1} components (X-ray amorphous phase) dissipated, whereas a band at 950 cm^{-1} appeared. It is of interest to point out that the ∼950 cm^{-1} component is directly related to the fluorine and/or Ag^{2+} content, as it was present in compositions fabricated with AgF_2 but not those fabricated with AgF.

3.2.4. Discussion on Raman Peaks 400−200 cm^{-1}. The Raman spectra in the low-frequency region were dominated by two weak peaks around 315 and 383 cm^{-1} ($x \leq 75$), which merged into a 340 cm^{-1} band at high AgF_x loading (80 mol %). The 383 cm^{-1} band was observed in all the spectra at mid AgF_x percentage and was independent of the oxidation state of the AgF_x precursor. Therefore, it can be assigned to the bending vibration of BX_6 octahedra. As for the 315 cm^{-1} peak, it was observed in the AgF_2-based samples and showed a systematic grow in intensity with AgF_2 content in the

(35) Kasinathan, D.; Kyker, A. B.; Singh, D. J. *Phys. Rev. B* **2006**, *73*, 214420.
(36) Grochala, W.; Egdell, R. G.; Edwards, P. P.; Mazej, Z.; Zemva, B. *ChemPhysChem.* **2003**, *4*, 997.
(37) Olorunyolemi, T.; Kydd, R. A. *Catal. Lett.* **2000**, *65*, 185.
(38) Christodoulakis, A.; Heracleous, E.; Lemonidou, A. A.; Boghosian, S. *J. Catal.* **2006**, *242*, 16.

precursor. Its absence in the AgF-based samples indicated that it may be related to the presence of $Mo^{4+}X_6$ octahedra as defined by the 925 cm^{-1} band. Increasing AgF_x loading to ~80 mol % resulted in the coalescence of the 315 and 383 cm^{-1} bands into a 340 cm^{-1} component. This shift can not be simply assigned to the vibration bond involving the shift of the bending band due to the substitution of Mo^{4+} for Mo^{6+} in light of its presence in the spectra with Mo^{6+} inducing AgF as a precursor. At this point, this peak remains undefined.

4. Electrochemical Characterization

Based on the formula $Ag_3MoO_3F_3$, it may be expected that a 3 electron silver displacement/reduction would occur at approximately 3 V. This would result in a capacity of 153 mA h/g and 954 mA h/cc and be followed by a two electron reduction of Mo^{6+} to Mo^{4+} at a lower voltage for a combined capacity of 255 and 1590 mA h/cc. Preliminary electrochemical evaluation of the AgF ($x = 0.7$)-based SMOF perovskite was performed on an SMOF electrode tape containing carbon black. As shown in Figure 13, the as-fabricated SMOF electrode tape has almost demonstrated full theoretical capacity when discharged to 1.5 V. The voltage profile reveals that the lithium insertion process initially developed with a plateau at approximately 3.6 V, consistent with the insertion of two Li^+. The third Li^+ most likely associated with the reduction of the third silver occurred at a lower voltage of 3.1 V. The final two lithium insertions associated with the reduction of Mo^{6+} to Mo^{4+} occurred around a plateau at 2.1 V in the voltage region of 2.5 to 1.5 V. The theoretical capacity of 255 mA h/g for the five-electron transfer was achieved.

A detailed in situ electrochemical study by XAS, Raman, and XRD was carried out. The full results of this study are beyond the scope/length of this paper; however, to shed some light on the reaction mechanism, the in situ XRD of the lithium insertion into SMOF (AgF ($x = 0.7$)) is shown in Figure 14. The angle range of the most intense Bragg peaks of SMOF around 2.9 Å was selected because this peak has minimum overlap with the system peaks (Be window, Al current collector, stainless steel holder) and is near the Ag Bragg reflection. Figure 14 shows the in situ XRD patterns of SMOF during discharge. Close examination of the in situ XRD results (Figure 14A) reveals that the perovskite peaks decrease in intensity as x in Li^+ increases from 0 to 3. This decrease in SMOF peak intensity is offset by an increase in intensity of the Bragg peak related to Ag^0 (111). By calculating the integrated intensity of SMOF peaks and Ag^0 (111), a systematic increase in Ag content up to $x = 3$ is clearly shown in Figure 15. For $x > 3$, there is little change in the intensity of the Ag^0 (111) peak (Figure 14B).These results are consistent with the displacement, or possible conversion reaction, of SMOF to Ag metal upon 3 lithium insertion at the first plateau (>3 V). Very little useful information has been obtained by in situ as to the development of the lithiation reaction at the output voltage below 3 V as the reacted phases have turned X-ray amorphous. These details will be discussed further with the use of in situ XAS and Raman in a following publication.

For practical applications, it will be ideal if proximity to theoretical capacity can be achieved without the addition of carbon in the electrode matrix, as this will retain the high volumetric capacity of the cathode. Therefore, we tested the electrochemical property of the pure SMOF perovskite with and without a small amount of carbon. The resulting voltage profiles of the SMOF (AgF, $x = 75$) perovskite are shown in Figure 16. All the samples were tested at a discharging rate of 7.58 mA/g. For electrodes containing no carbon black, the preliminary electrochemical data of the SMOF perovskite have revealed a high average output voltage of ~3.4 V at the first plateau (>3 V) and a good total specific capacity of ~170 mA h/g between 4 and 2 V. The electrode with carbon resulted in a smaller degree of polarization with no significant improvement in the total capacity.

On the basis of the density (6.177 g/cc) obtained by He pycnometry, a very high volumetric energy density of ~ 2570 W h/L was achieved at the first plateau (>3 V) for the SMOF material shown in Figure 13. The overall volumetric energy density between 4 and 1.5 V was calculated to be ~4470 W h/L. The detailed electrochemical data of the as-fabricated SMOF perovskite are present in Table 4, showing that the silver molybdenum oxyfluoride perovskites have a much higher energy density than that of silver vanadium oxide (SVO), the state of the art, in the more desirable 3 V range. Therefore, such material offers an interesting avenue of research as alternative high-energy-density primary electrodes.

5. Summary

Novel perovskite-type silver molybdenum oxyfluorides have been successfully synthesized through the use of mechanochemistry by high-energy-milling mixtures of AgF or AgF_2, MoO_3, and MoO_2. Refinement by Rietveld analysis indicated that the perovskite phase was associated with the monoclinic cryolite of space group $P2_1/n$, which was consistent with the observation of the allowed Raman bands. The most intense XRD and Raman spectra corresponded with the ideal $P2_1/n$ composition $Ag^{1+}{}_3Mo^{6+}(O_3F_3)$. At high fluorination composition, the substitution of Mo^{4+} on the B site and an assumed stoichiometric modulation of the oxyfluoride anion composition were supported by XRD and Raman analysis.

The SMOF perovskites demonstrated good electronic conductivity and promising electrochemical activity as cathodes even without the presence of carbon black for lithium batteries. At this early point, the investigated compositions have led to overall energy densities on par with today's state of the art materials but energy densities above 3 V that are much improved. The as-fabricated SMOF perovskite based on $Ag^+{}_3Mo^{6+}(O_3F_3)$ is expected to exhibit a theoretical specific capacity of 153 mA h/g ($3e^-$ transfer) and a volumetric capacity of 954 A h/L in the important voltage region above 3V.

Acknowledgment. The authors thank Greatbatch for its support of this research. The authors also thank F. Badway, N. Pereira, I. Plitz, J. Gural, A. DuPasquier, and P. Barpanda for their technical assistance.

CM803322D